

Sensitivity of Multi-Particle Azimuthal Correlations and Rapidity-Even Dipolar flow to α -Clustering in O+O Collisions at $\sqrt{s_{NN}} = 200$ GeV

Kaiser Shafi
and
Dr. Sandeep Chatterjee

Department of Physical Sciences,
Indian Institute of Science Education and Research, Berhampur
[arXiv:2505.11713](https://arxiv.org/abs/2505.11713)

September 4, 2025
Hot QCD Matter 2025



- ① Introduction
- ② Heavy-ion Collisions Dynamics
- ③ Simulation Framework
- ④ Observables
- ⑤ Results and Discussion
- ⑥ Summary

1 Introduction

2 Heavy-ion Collisions Dynamics

3 Simulation Framework

4 Observables

5 Results and Discussion

6 Summary

Introduction to anisotropic flow

Initial anisotropy in coordinate space

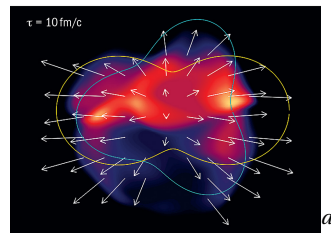
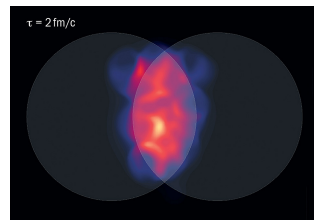


Thermalized medium



Final anisotropy in momentum space

Anisotropic flow is a sensitive probe both of initial conditions in heavy-ion collisions, and of QGPs transport properties (e.g. shear viscosity).



^a<https://cerncourier.com/a/going-with-the-flow>

Challenge in Separating Initial State and Transport Properties

- Traditional observables mix contributions from initial state and medium dynamics.
- Need for observables that isolate sensitivity to initial-state properties (e.g., nuclear geometry and fluctuations) and transport dynamics (e.g., shear and bulk viscosity).
- Goal: Provide more direct constraints on initial state and medium properties.

1 Introduction

2 Heavy-ion Collisions Dynamics

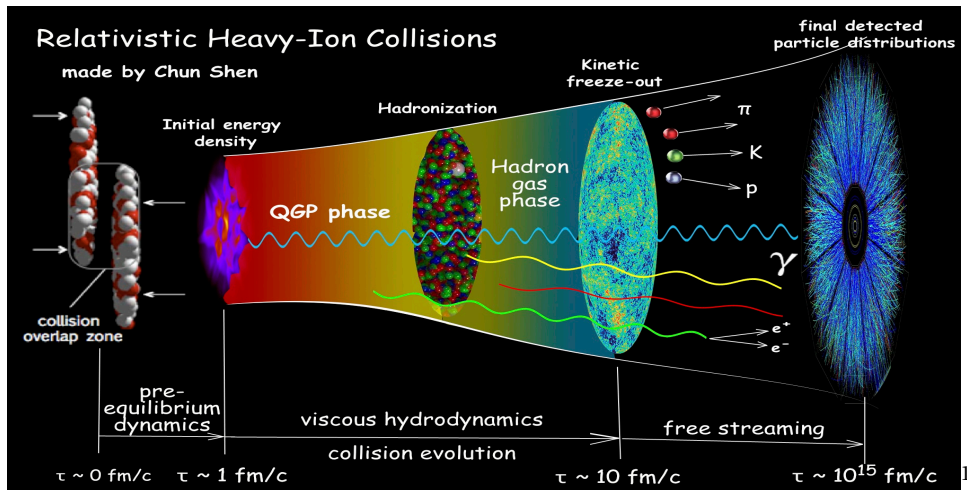
3 Simulation Framework

4 Observables

5 Results and Discussion

6 Summary

Heavy-ion Collisions Dynamics



¹Chun Shen: <https://chunshen1987.github.io/>

1 Introduction

2 Heavy-ion Collisions Dynamics

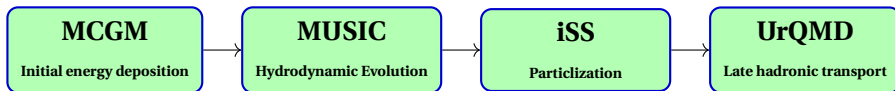
3 Simulation Framework

4 Observables

5 Results and Discussion

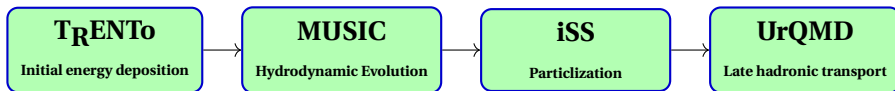
6 Summary

Simulation Framework



- $s(x, y) \propto (1 - \alpha) n_{\text{part}}(x, y) + \alpha n_{\text{coll}}(x, y)$
- $\partial_{\mu} T^{\mu\nu} = 0$
- $E \frac{dN_i}{d^3p} = \frac{dN_i}{p_T dp_T dy d\phi} = \frac{2S+1}{(2\pi)^3} \int_{\Sigma} \frac{1}{e^{\frac{p_{\mu} u^{\mu} - (\mu_B)_{fB_i}}{T_f} \pm 1}} p^{\mu} \Delta\sigma_{\mu}$
- $p^{\mu} \partial_{\mu} f(x, p) = C[f]$

Simulation Framework



- $s(x, y) \propto \sqrt{T_A T_B}$, $T_{A,B}(x, y) = \int dz \rho_{A,B}^{\text{part}}(x, y, z)$.
- $\partial_\mu T^{\mu\nu} = 0$
- $E \frac{dN_i}{d^3 p} = \frac{dN_i}{p_T dp_T dy d\phi} = \frac{2S+1}{(2\pi)^3} \int_\Sigma \frac{1}{e^{\frac{p_\mu u^\mu - (\mu_B) f^{B_i}}{T_f} \pm 1}} p^\mu \Delta \sigma_\mu$
- $p^\mu \partial_\mu f(x, p) = C[f]$

- ① Introduction
- ② Heavy-ion Collisions Dynamics
- ③ Simulation Framework
- ④ Observables**
- ⑤ Results and Discussion
- ⑥ Summary

Fourier decomposition of initial state energy density

We perform Fourier decomposition of the energy density profile in the following way:

$$\varepsilon_n e^{in\psi_n^{PP}} = -\frac{\langle r^n e^{in\phi} \rangle}{\langle r^n \rangle}; \quad \langle \dots \rangle = \frac{\int \dots e(r, \phi) r dr d\phi}{\int e(r, \phi) r dr d\phi} \quad (1)$$

where ε_n is the n^{th} order eccentricity and ψ_n^{PP} is the n^{th} order participant plane².

Linear response:

$$v_2 = k_2 \varepsilon_2$$

$$v_3 = k_3 \varepsilon_3$$

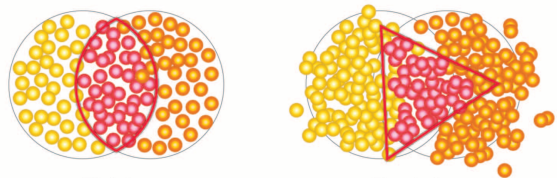


Figure 1: Ellipticity (left) and triangularity (right) arise from the locations of individual nucleons at the instant when two nuclei interpenetrate. The nucleons of one nucleus are shown in yellow and the other in orange. Red indicates those nucleons in the overlap region, which actually collide.

²Müller et al. Science 337, 310 (2012)

Definition of flow

Fourier decomposition of single-particle momentum distribution:

$$f(\mathbf{p}) = E \frac{d^3 N}{d^3 \mathbf{p}} = \frac{1}{2\pi} \frac{d^2 N}{p_T dp_T dy} \left[1 + 2 \sum_{n=1}^{\infty} v_n e^{in\phi} \right] \quad (2)$$

$$v_n(\mathcal{D}) \equiv \langle e^{in\phi} \rangle = \frac{\int_{\mathcal{D}} e^{in\phi} f(\mathbf{p}) d^3 \mathbf{p}}{\int_{\mathcal{D}} f(\mathbf{p}) d^3 \mathbf{p}}, \quad (3)$$

where the brackets denote an average value over many events, and \mathcal{D} represents a phase space window in the (p_T, y) plane where flow is measured. Anisotropic flow is quantified with v_n :

- v_1 : directed flow
- v_2 : elliptic flow
- v_3 : triangular flow
- v_4 : quadrangular flow, etc.

Symmetric Cumulants

- **Symmetric Cumulants** (SCs) are used to measure correlations between event-by-event fluctuations of flow harmonics v_m and v_n .
- This approach allows separation of non-flow and flow contributions, providing insights into how the combinatorial background affects flow measurements using correlation techniques.

The four-particle symmetric cumulants, $SC(m, n)$, are defined as³

$$\begin{aligned}
 SC(m, n) &\equiv \langle v_m^2 v_n^2 \rangle_c \\
 &= \langle v_m^2 v_n^2 \rangle - \langle v_m^2 \rangle \langle v_n^2 \rangle \\
 &= \langle \langle \cos(m\varphi_1 + n\varphi_2 - m\varphi_3 - n\varphi_4) \rangle \rangle \\
 &\quad - \langle \langle \cos[m(\varphi_1 - \varphi_2)] \rangle \rangle \langle \langle \cos[n(\varphi_1 - \varphi_2)] \rangle \rangle
 \end{aligned} \tag{4}$$

The subscript c indicates the cumulant.

³ (Phys. Rev. C 89, 064904 (2014))

Asymmetric Cumulants

Generalization of these observables to probe the genuine correlation between different moments of flow harmonics. The **Asymmetric Cumulants** $AC_{2,1}(m, n)$ is defined as:⁴

$$\begin{aligned} AC_{2,1}(m, n) &\equiv \langle (v_m^2)^2 v_n^2 \rangle_c \equiv \langle v_m^4 v_n^2 \rangle_c \\ &= \langle v_m^4 v_n^2 \rangle - \langle v_m^4 \rangle \langle v_n^2 \rangle - 2 \langle v_m^2 v_n^2 \rangle \langle v_m^2 \rangle + 2 \langle v_m^2 \rangle^2 \langle v_n^2 \rangle \end{aligned} \quad (5)$$

In terms of azimuthal correlators:

$$\begin{aligned} AC_{2,1}(m, n) &= \langle \langle e^{i(m\varphi_1 + m\varphi_2 + n\varphi_3 - m\varphi_4 - m\varphi_5 - n\varphi_6)} \rangle \rangle \\ &\quad - \langle \langle e^{i(m\varphi_1 + m\varphi_2 - m\varphi_3 - m\varphi_4)} \rangle \rangle \langle \langle e^{i(n\varphi_1 - n\varphi_2)} \rangle \rangle \\ &\quad - 2 \langle \langle e^{i(m\varphi_1 + n\varphi_2 - m\varphi_3 - n\varphi_4)} \rangle \rangle \langle \langle e^{i(m\varphi_1 - m\varphi_2)} \rangle \rangle \\ &\quad + 2 \langle \langle e^{i(m\varphi_1 - m\varphi_2)} \rangle \rangle^2 \langle \langle e^{i(n\varphi_1 - n\varphi_2)} \rangle \rangle \end{aligned} \quad (6)$$

$AC_{1,1}(m, n) \equiv SC(m, n)$, \implies Generalization aspect of ACs.

⁴ (Phys. Rev. C 105, 024912 (2022))

Normalized Cumulants

To eliminate the effect of the magnitudes of v_m and v_n on the value of the symmetric cumulant, we divide $SC(m, n)$ by their average values, $\langle v_m^2 \rangle$ and $\langle v_n^2 \rangle$.

- Normalization enables fair comparison of initial and final states.
- Normalization removes dependence on p_T ranges across models and data.

The normalized symmetric cumulant, denoted by $NSC(m, n)$, is defined as⁵:

$$NSC(m, n) = \frac{SC(m, n)}{\langle v_m^2 \rangle \langle v_n^2 \rangle}. \quad (7)$$

Normalized asymmetric cumulants are defined as:

$$NAC_{2,1}(m, n) = \frac{AC_{2,1}(m, n)}{\langle v_m^2 \rangle^2 \langle v_n^2 \rangle}. \quad (8)$$

⁵ (Eur. Phys. J. C 81, 652 (2021))

1 Introduction

2 Heavy-ion Collisions Dynamics

3 Simulation Framework

4 Observables

5 Results and Discussion

Identifying Observables Sensitive to Initial and Final States
Constraining Oxygen Nuclear Distribution

6 Summary

1 Introduction

2 Heavy-ion Collisions Dynamics

3 Simulation Framework

4 Observables

5 Results and Discussion

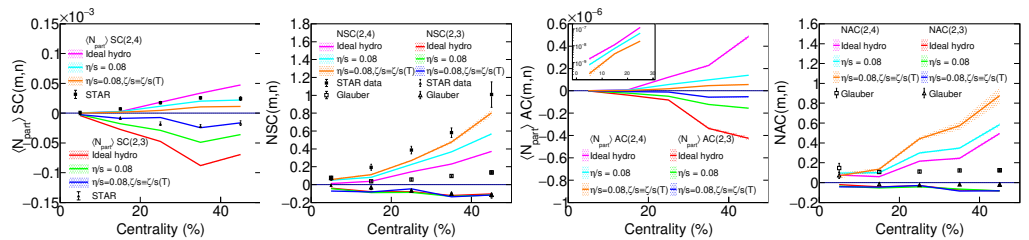
Identifying Observables Sensitive to Initial and Final States
Constraining Oxygen Nuclear Distribution

6 Summary

Probing QGP transport properties: $^{197}\text{Au}+^{197}\text{Au}$ Collisions

- Analyze multi-particle correlations to assess sensitivity to QGP transport coefficients (shear, bulk viscosity) and late-stage hadronic interactions.
- Identify observables sensitive to initial-state and insensitive to the transport properties.
- Role of normalized cumulants in probing the initial state across RHIC and LHC energies.

Sensitivity of Symmetric and Asymmetric Cumulants to QGP Transport Coefficients



- Model vs STAR data⁶.
- The large sensitivity of symmetric and asymmetric cumulants primarily arises from the characteristics of anisotropic flow, as the symmetric cumulants involve higher powers of flow coefficients.
- $v_2 - v_3$ correlations: Hydro = Glauber. $v_2 - v_4$ correlations: Hydro \neq Glauber.
- NSC(2,3) and NAC_{2,1}(2,3) are insensitive to the hydro model parameters and late-stage hadronic interactions. Reliable for constraining the initial state of the system's evolution.
- NSC(2,4) and NAC_{2,1}(2,4) show considerable sensitivity to these dynamics.

⁶ (PhysRevC.111.064901 (2024)), (Phys. Lett. B 783, 459 (2018))



1 Introduction

2 Heavy-ion Collisions Dynamics

3 Simulation Framework

4 Observables

5 Results and Discussion

Identifying Observables Sensitive to Initial and Final States
Constraining Oxygen Nuclear Distribution

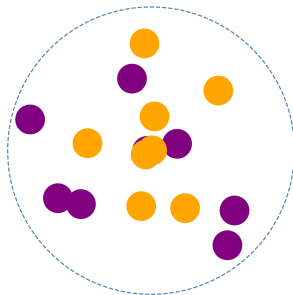
6 Summary

Probing Nuclear Structure: $^{16}\text{O} + ^{16}\text{O}$ Collisions

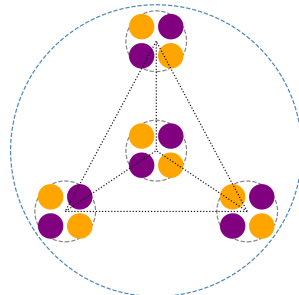
- Simulate $^{16}\text{O} + ^{16}\text{O}$ collisions using Woods-Saxon and α -clustered configurations.
- Investigate effects of nuclear deformation and α -clustering on final-state observables.
- Key observables: Symmetric and Asymmetric cumulants, and rapidity-even dipolar flow v_1^{even} .

Probing Nuclear Structure: $^{16}\text{O}+^{16}\text{O}$ Collisions

Non-clustered Oxygen (^{16}O) nucleus
with Woods-Saxon distribution



α -clustered Oxygen (^{16}O) nucleus



● Proton ● Neutron --○-- α -particle

Figure 2: Pictorial representation of a non-clustered (left) and α -clustered (right) distribution of nucleons inside the ^{16}O nucleus.

Nuclear distributions

Woods-Saxon distribution:

$$\rho = \rho_0 \left(1 + \omega r^2 / R^2\right) \left[1 + \exp((r - R)/a)\right]^{-1}$$

We impose that the root-mean-square radius of ^{16}O should be the same for the different densities, i.e.,

$$\sqrt{\langle r^2 \rangle} \equiv \sqrt{\frac{3l^2}{8} + r_\alpha^2} = 2.73 \text{ fm},$$

which is taken from nuclear structure experiments.⁹

	Distribution	R	a	ω
WS	Woods-Saxon	2.608 fm	0.513 fm	-0.051
		l	r_α	r_α/l
Cl. I	α cluster	3.0	2.0	0.67
Cl. II	α cluster	3.6	1.6	0.44
Cl. III	α cluster	4.0	1.2	0.30

Table 1: The parameters for the nuclear distributions of ^{16}O with Woods-Saxon and tetrahedral configurations of α clusters.

⁹ (Atom. Data Nucl. Data Tabl. 36, 495 (1987))

Nuclear distributions

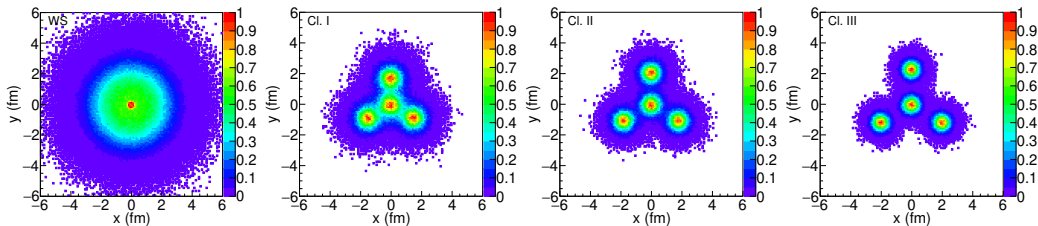
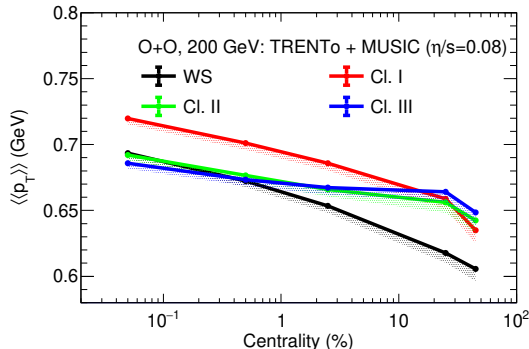


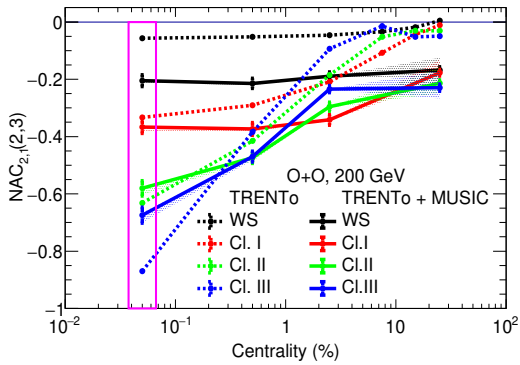
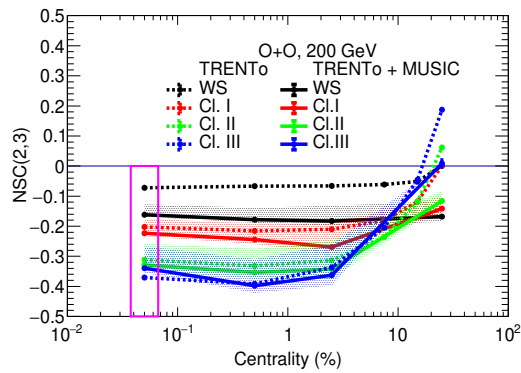
Figure 3: Nuclear distributions of ^{16}O using Woods-Saxon and tetrahedral α -cluster configurations.

Mean transverse momentum



- Bands represent systematic uncertainties from η/s .
- $\langle\langle p_T \rangle\rangle$ decreases with Centrality due to reduced medium response.
- In ultra-central collisions, $\langle\langle p_T \rangle\rangle$ drops as α clusters become more compact, due to incoherent flow from different hotspots.
- In mid-central collisions, the hierarchy reverses, with collisions occurring between α clusters, not the whole nuclei.

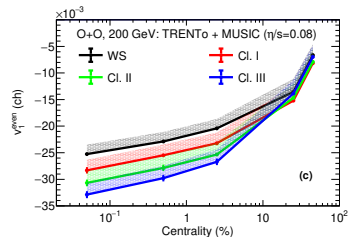
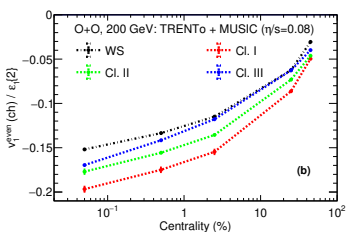
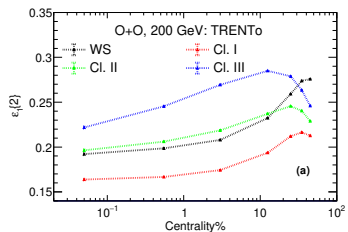
NSC(2,3) and NAC_{2,1}(2,3)



- Dashed lines: TRENTo, Solid lines: TRENTo+MUSIC.
- Bands show systematic uncertainties, dominated by ζ/s .
- Notable distinction among nuclear configurations in ultra-central collisions, especially from AC_{2,1}(2,3).



Rapidity-even dipolar flow¹⁰



- $\varepsilon_1\{2\}$ increases with cluster compactness due to fewer effective sources in compact clustered nucleus.
- Response, $v_1^{even}/\varepsilon_1\{2\}$, decreases with centrality and increasing compactness.
- In ultra-central collisions, the v_1^{even} hierarchy is dominated by $\varepsilon_1\{2\}$.
- Distinction among nuclear configurations in ultra-central collisions from v_1^{even} .

¹⁰Phys. Rev. Lett. 106, 102301 (2011)

- ① Introduction
- ② Heavy-ion Collisions Dynamics
- ③ Simulation Framework
- ④ Observables
- ⑤ Results and Discussion
- ⑥ Summary**

Summary

- We studied symmetric and asymmetric cumulants, and rapidity-even dipolar flow in $^{16}\text{O} + ^{16}\text{O}$ collisions at $\sqrt{s_{NN}} = 200$ GeV using viscous relativistic hydrodynamics.
- **Normalized cumulants** $\text{NSC}(2,3)$ and $\text{NAC}_{2,1}(2,3)$, based on $v_2 - v_3$ correlations, **are insensitive to hydrodynamic parameters and late-stage hadronic interactions**, making them reliable for constraining the initial state.
- Provides new methods for **isolating initial-state and medium dynamics**.
- We identified that **final-state symmetric and asymmetric cumulants, $\text{NSC}(2,3)$ and $\text{NAC}_{2,1}(2,3)$, are sensitive to the initial nuclear geometry**.
- Observed a **significant difference in rapidity-even dipolar flow, v_1^{even}** , between α -clustered and WoodsSaxon configurations **in high-multiplicity events**.
- The magnitude and centrality dependence of the **normalized cumulants show** similar trends at both ALICE and STAR, suggesting **minimal energy dependence**.

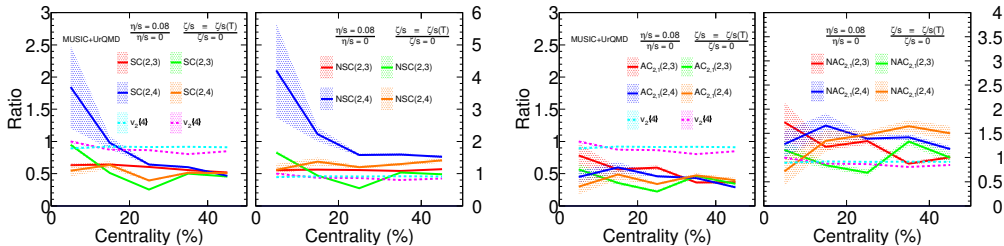
Thank you for your attention!

Kaiser Shafi

kaisers@iiserbpr.ac.in

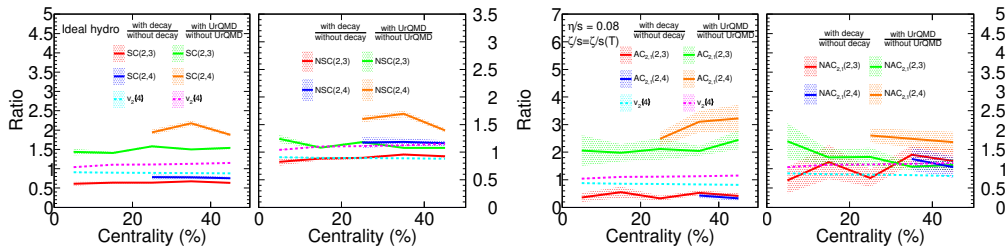
Backup Slides

Sensitivity of Symmetric and Asymmetric Cumulants to QGP Transport Coefficients



- The large sensitivity of symmetric and asymmetric cumulants primarily arises from the characteristics of anisotropic flow, as the symmetric cumulants involve higher powers of flow coefficients.
- NSC(2,3) and $NAC_{2,1}(2,3)$ are insensitive to the hydro model parameters. Reliable for constraining the initial state of the system's evolution.
- NSC(2,4) and $NAC_{2,1}(2,4)$ show considerable sensitivity to these parameters, allowing them to effectively constrain hydrodynamic models.

Sensitivity of Symmetric and Asymmetric Cumulants to Resonance Decays and Hadronic Interactions



- The large sensitivity of symmetric and asymmetric cumulants primarily arises from the characteristics of anisotropic flow, as the symmetric cumulants involve higher powers of flow coefficients.
- NSC(2,3) and NAC_{2,1}(2,3) are insensitive to late-stage hadronic interactions. Reliable for constraining the initial state of the systems evolution.
- NSC(2,4) and NAC_{2,1}(2,4) show considerable sensitivity to these stages, allowing them to effectively constrain transport models.

Sensitivity of Asymmetric Cumulants to Resonance Decays and Hadronic Interactions

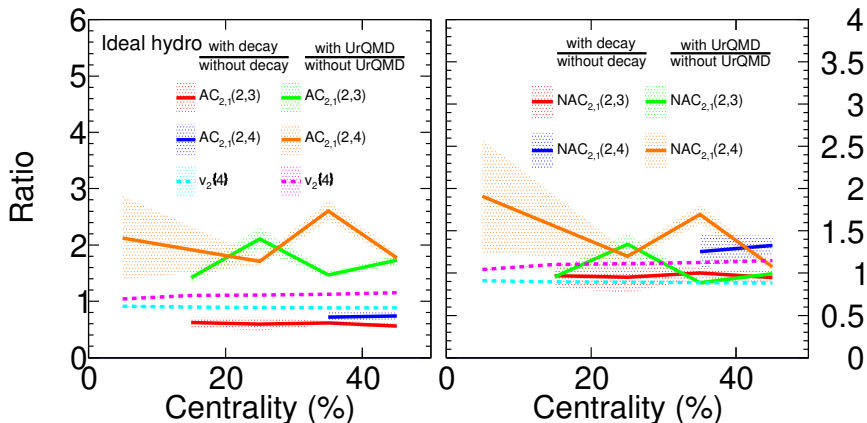


Figure 4: Ratios of $v_2\{4\}$, $AC_{2,1}(2, n)$, and $NAC_{2,1}(2, n)$, computed at the three different stages of the evolution, vs centrality in Au+Au collisions at $\sqrt{s_{NN}} = 200$ GeV.

Sensitivity of Symmetric Cumulants to Resonance Decays and Hadronic Interactions

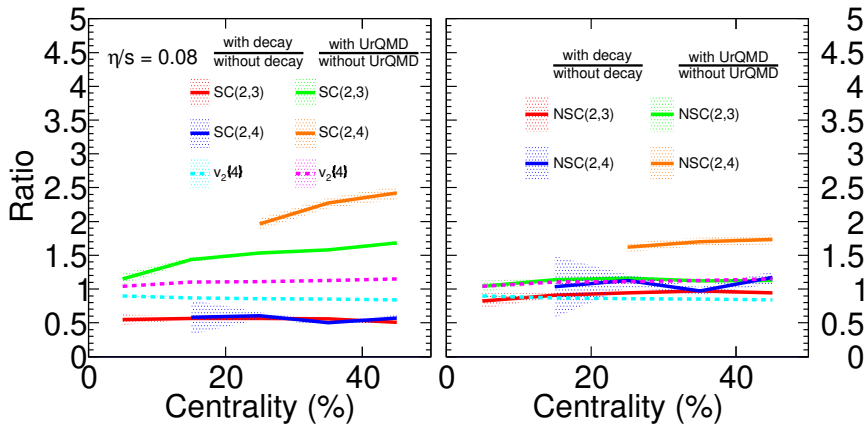


Figure 5: Ratios of $v_2\{4\}$, $SC(2, n)$, and $NSC(2, n)$, computed at the three different stages of the evolution, vs centrality in Au+Au collisions at $\sqrt{s_{NN}} = 200$ GeV.

Sensitivity of Asymmetric Cumulants to Resonance Decays and Hadronic Interactions

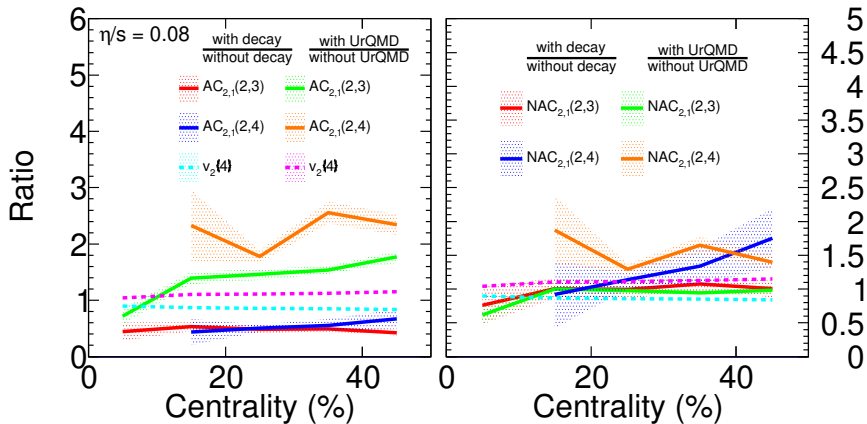


Figure 6: Ratios of $v_2\{4\}$, $AC_{2,1}(2, n)$, and $NAC_{2,1}(2, n)$, computed at the three different stages of the evolution, vs centrality in Au+Au collisions at $\sqrt{s_{NN}} = 200$ GeV.

Sensitivity of Symmetric Cumulants to Resonance Decays and Hadronic Interactions

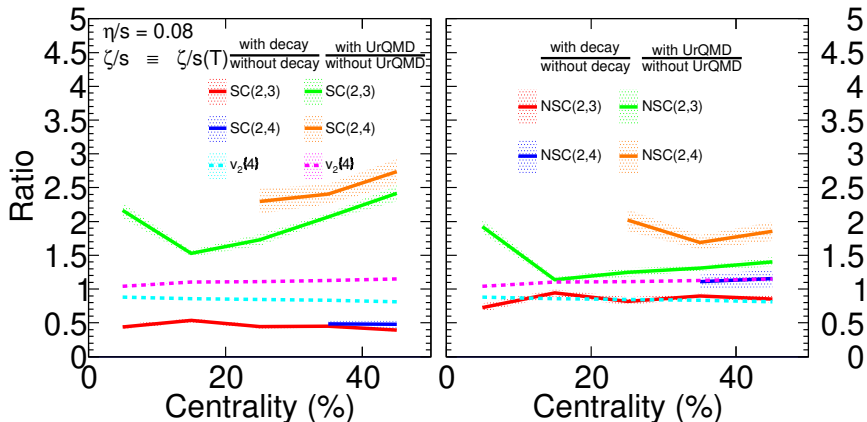


Figure 7: Ratios of $v_2\{4\}$, $SC(2, n)$, and $NSC(2, n)$, computed at the three different stages of the evolution, vs centrality in Au+Au collisions at $\sqrt{s_{NN}} = 200$ GeV.